Laboratory Investigation (2006) 86, 175–190

www.laboratoryinvestigation.org

Evidence for alternative candidate genes near *RB1* involved in clonal expansion of *in situ* urothelial neoplasia

Mi-Sook Kim[1,*], Joon Jeong[1,*], Tadeusz Majewski[1], Andrzej Kram[1], Dong-Sup Yoon[1], Ruo-Dan Zhang[1], Jun-Zhi Li[1], Konrad Ptaszynski[1], Tang C Kuang[2], Jain-Hua Zhou[3], Ubaradka G Sathyanarayana[4], Tomasz Tuziak[1], Dennis A Johnston[2], Herbert B Grossman[5], Adi F Gazdar[4], Steven E Scherer[6], William F Benedict[3] and Bogdan Czerniak[1]

[1]*Department of Pathology, The University of Texas MD Anderson Cancer Center, Houston, TX, USA;* [2]*Department of Biomathematics, The University of Texas MD Anderson Cancer Center, Houston, TX, USA;* [3]*Department of Genitourinary Medical Oncology, The University of Texas MD Anderson Cancer Center, Houston, TX, USA;* [4]*University of Texas Southwestern Medical Center, Dallas, TX, USA;* [5]*Department of Urology, The University of Texas MD Anderson Cancer Center, Houston, TX, USA and* [6]*Human Genome Sequencing Center, Baylor College of Medicine, Houston, TX, USA*

In this paper, we present whole-organ histologic and genetic mapping studies using hypervariable DNA markers on chromosome 13 and then integrate the recombination- and single-nucleotide polymorphic sites (SNPs)-based deletion maps with the annotated genome sequence. Using bladders resected from patients with invasive urothelial carcinoma, we studied allelic patterns of 40 microsatellite markers mapping to all regions of chromosome 13 and 79 SNPs located within the 13q14 region containing the *RB1* gene. A whole-organ histologic and genetic mapping strategy was used to identify the evolution of allelic losses on chromosome 13 during the progression of bladder neoplasia. Markers mapping to chromosomal regions involved in clonal expansion of preneoplastic intraurothelial lesions were subsequently tested in 25 tumors and 21 voided urine samples of patients with bladder cancer. Four clusters of allelic losses mapping to distinct regions of chromosome 13 were identified. Markers mapping to the 13q14 region that is flanked by D13S263 and D13S276, which contains the *RB1* gene, showed allelic losses associated with early clonal expansion of intraurothelial neoplasia. Such losses could be identified in approximately 32% bladder tumor tissue samples and 38% of voided urines from patients with bladder cancer. The integration of distribution patterns of clonal allelic losses revealed by the microsatellite markers with those obtained by genotyping of SNPs disclosed that the loss within an approximately 4-Mb segment centered around *RB1* may represent an incipient event in bladder neoplasia. However, the inactivation of *RB1* occurred later and was associated with the onset of severe dysplasia/carcinoma *in situ*. Our studies provide evidence for the presence of critical alternative candidate genes mapping to the 13q14 region that are involved in clonal expansion of neoplasia within the bladder antecedent to the inactivation of the *RB1* gene.
Laboratory Investigation (2006) **86,** 175–190. doi:10.1038/labinvest.3700378; published online 9 January 2006

Keywords: SNP-based mapping; *in situ* neoplasia; alternative candidate genes near *RB1*; bladder *in situ* neoplasia; *RB1* locus

Recent studies provide evidence that many common epithelial cancers, including those arising in the bladder, begin as clonal *in situ* expansion of neoplastic cells, which show no or minimal deviation from the normal phenotype.[1–4] Such lesions often form plaques involving large areas of the affected mucosa and their expansion precedes the development of microscopically recognizable dysplasia or *carcinoma in situ*.[4,5] Identification of chromosomal regions associated with the initial expansion of neoplasia is a requisite for future identification of their positional candidate genes that may provide growth advantage for a neoplastic clone.

Correspondence: Dr B Czerniak, MD, PhD, Department of Pathology, The University of Texas MD Anderson Cancer Center, Box 085, 1515 Holcombe Boulevard, Houston, TX 77030, USA.
E-mail: bczernia@mdanderson.org
*These authors contributed equally to this study
Received 12 October 2005; revised 11 November 2005; accepted 12 November 2005; published online 9 January 2006

We have previously reported the identification of several chromosomal regions involved in early clonal expansion of bladder neoplasia and constructed a genetic model of bladder cancer development from occult intraurothelial precursor lesions.[6–10] These studies utilized a whole-organ histologic and genetic mapping approach with microsatellite markers and low-resolution recombination-based chromosomal maps. More recently, we have reported on whole-organ histologic and genetic mapping of tumor suppressor gene loci using single-nucleotide polymorphic sites (SNPs).[11] These studies provided evidence that a combined whole-organ histologic and genetic mapping with SNPs can provide valuable information on sequential hits in early occult phases of human carcinogenesis.

Here, we report the results of our studies on the evolution of losses on chromosome 13 in the progression of bladder neoplasia from *in situ* precursor conditions to invasive disease. Bladder cancer was selected since it is a good human tumor model for studies of early events in carcinogenesis due to its simple anatomy and the ease in mapping *in situ* neoplastic lesions across the entire mucosa.[12–14]

In this paper, we present whole-organ histologic and genetic mapping studies using hypervariable DNA markers on chromosome 13 and then integrate the recombination-based deletion maps with physical and genome sequence maps. Subsequently, the high-resolution mapping of the *RB1* region by genotyping of SNPs is described. Finally, we present the integration of allelic losses in 13q14 with *RB1* sequencing, methylation status of its promoter, and RB1 protein expression patterns in bladder mucosa. Using this approach, it has been possible to identify the pattern of *RB1* involvement in the development of bladder cancer and perhaps even more significant provide evidence that genes near *RB1* rather than *RB1* itself are involved in the initial *in situ* expansion of a neoplastic clone.

Materials and methods

Tumor Tissues and Voided Urine Samples

Whole-organ histologic and genetic mapping of chromosome 13 was performed on radical cystectomy specimens from eight patients (seven males and one female) with untreated sporadic high-grade (grade 3) invasive transitional cell carcinoma (TCC) of the bladder. Their ages ranged from 47 to 82 years (mean = 64.75 ± 13.1 s.d.). Subsequently, markers mapping to deleted regions identified by whole-organ mapping as well as their flanking markers with retention of heterozygosity were tested on DNA extracted from 25 frozen tumors and 21 voided urine samples of patients with TCC. Urine samples were collected before cystoscopy and the presence of tumor was verified by pathologic examination of intracystoscopically resected tumor tissue. The precursor *in situ* lesions and tumor samples were microscopically classified as described previously.[5–10] In brief, the intraurothelial precancerous changes were classified as mild, moderate, or severe dysplasia or as carcinoma *in situ*. For the purpose of statistical analyses, the intraurothelial precancerous changes were classified into two major groups: low-grade intraurothelial neoplasia (LGIN, mild and moderate dysplasia) and high-grade intraurothelial neoplasia (HGIN, severe dysplasia and carcinoma *in situ*) as described previously.[11] The TCCs were classified according to the three-tier histologic grading system of the World Health Organization histologic grading system, and growth pattern (papillary *vs* nonpapillary).[15] The depth of invasion was recorded according to TNM (tumor-node metastasis) staging system.[16] Stage T_1 (lamina propria invasion) has been divided into T_{1a} (no muscularis mucosae invasion) and T_{1b} (muscularis mucosae invasion), which have a clinically significantly higher risk of progression.[17] Consequently, the tumors were dichotomized into superficial (T_a–T_{1a}) and invasive (T_{1b} and higher) groups as described previously.[18] DNA was extracted from individual bladder tumors and sediments of voided urine samples as described previously.[9] For controls, DNA was also extracted from the peripheral blood lymphocytes and/or normal nonbladder tissue in the resected specimens from each patient.

Whole-Organ Histologic and Genetic Mapping

Whole-organ histologic and genetic mapping was performed as described in our previous publications.[6–10] In brief, each fresh cystectomy specimen was opened longitudinally along the anterior wall of the bladder and pinned down to a paraffin block. The entire mucosa was divided into 1×2 cm rectangular samples and evaluated microscopically on frozen sections. The tissue of interest was microdissected from the frozen block and cell suspensions were prepared by mechanically scraping the urothelial mucosa or gently shaking invasive tumor samples. Only those specimens that yielded more than 90% of microscopically recognizable intact urothelial, dysplastic, or tumor cells in each sample were accepted for the study and used for DNA extraction. This procedure provided 49, 39, 65, 42, 39, 30, 33, and 49 DNA samples from each of the cystectomy specimens that corresponded to microscopically identified intraurothelial precursor conditions or invasive carcinoma.

In seven of the eight cystectomy specimens, a single focus of grade 3 nonpapillary urothelial carcinoma invaded the muscularis propria and was accompanied by extensive precancerous lesions ranging from mild dysplasia to carcinoma *in situ*. In the remaining case, multiple foci of carcinoma were present. One focus represented a grade 3 nonpapillary urothelial carcinoma with transmural

invasion of the bladder wall and involvement of perivesical adipose tissue. Two additional foci of carcinoma represented grade 3 papillary urothelial carcinoma without invasion. Like the other seven cases, this case exhibited changes ranging from mild dysplasia to carcinoma *in situ* over extensive areas of the urinary bladder mucosa. The results of microscopic evaluation of individual samples from eight cystectomy specimens were recorded and stored in a computer database as histologic maps.

Microsatellite Marker Analysis and Gene Candidate Identification

The analysis of microsatellite markers and the integration of recombination-based deletion map of chromosome 13 with the physical maps and the human genome sequence was performed as described previously.[9,10] In brief, a set of primers for 40 microsatellite markers on chromosome 13 based on the sex-averaged microsatellite maps from Genethon and Marshfield using reference families from the Cooperative Human Linkage Center was obtained from Research Genetics (Huntsville, AL, USA; now Invitrogen, CA, USA). The allelic patterns of markers were resolved on 6% polyacrylamide gels after polymerase chain reaction (PCR) amplification. A minimum 50% reduction in signal intensity was required to be considered evidence of loss of heterozygosity (LOH).

During the course of this study, the mapping, genome sequence, and annotation resources available underwent a rapid evolution. An elaborate integration strategy was necessary to move from the genetic recombination-based microsatellite map to the genome sequence. These efforts can now be accomplished by finding the marker coordinates on the latest build of the human genome available via either the UCSC Genome Browser or Ensembl genome browser (http://genome.ucsc.edu/ or http://www.ensembl.org, respectively) and then using the Vertebrate Genome Annotation browser (http://vega.sanger.ac.uk/) to scan the region for genes and gene predictions.

Genotyping with SNPs

Whole-organ genotype with SNPs was performed as described previously.[10] In brief, the positions of all currently defined SNPs mapping within the 13q14 region from the SNP database of NCBI (http://www.ncbi.nlm.nih.gov/SNP) were integrated with the genome sequence map containing genes and gene predictions. The integrated gene and SNP map of the region was used to select 79 SNPs mapping within the approximately 800 kb segment around *RB1*, which included 30 SNPs located within the *RB* gene. The genotyping of SNPs was performed by pyrosequencing methods.[19,20] For pyrosequencing, genomic DNA fragments containing SNPs were amplified by PCR with one of each primer biotinylated at the 5′-end. Single, stranded DNA was isolated by streptavidin-coated magnetic beads (Dynabeads M-280, Dynal, Oslo, Norway). The sequencing reaction mixture contained the single-stranded DNA with sequencing primer annealed, DNA polymerase, apyrase, luciferase, ATP sulfurylase, adenosine 5′-phosphosulfate, and luciferin. Genotyping of SNPs was performed using an automatic pyrosequencing instrument PSQ™ 96 MA (Pyrosequencing AB, Uppsala, Sweden). The sequence was determined from the measured signal output of light upon nucleotide incorporation. The resulting peaks were analyzed using pyrosequencing software. A minimum of 50% of signal intensity reduction from one of the polymorphic nucleotides was used to identify allelic loss. Genotyping of SNPs was performed in three sequential steps. Initially, all selected SNPs of normal genomic DNA were sequenced. In the next steps, those SNPs that exhibited polymorphism were tested on paired normal-invasive tumor DNA samples of the same patient. In the final step, those SNPs that showed allelic loss were tested on all mucosal samples of the same cystectomy specimen. The distribution of clonal allelic losses of each SNP were subsequently superimposed over the histologic map of the entire organ and integrated with the distribution patterns of clonal allelic losses identified by the hypervariable DNA markers.

Sequencing of *RB1* Gene

The 27 exons of *RB1* were amplified and directly sequenced by applying the Taq cycle sequencing dye terminator protocol. PCR products were purified from unincorporated primers and dNTPs by using exonuclease I and shrimp alkaline phosphatase. Sequencing reactions were analyzed with an ABI 3730 sequencer (Applied Biosystems, Foster City, CA, USA). Sequencing was repeated with primers of reverse direction. Initially, all 27 exons of *RB1* were sequenced on representative DNA samples corresponding to invasive TCC of each cystectomy. Subsequently, those exons, which showed mutations, were sequenced on all mucosal samples of the same cystectomy, and the distribution patterns of the mutations were superimposed over histologic maps of their cystectomy specimens.

Immunohistochemical Analysis of RB1 Protein Expression

RB1 protein status was determined by immunohistochemical analysis of frozen sections using the RB-WL-1 polyclonal anti-RB antibody as described previously.[21–23] RB-WL-1 is a rabbit polyclonal antibody produced against a peptide encoded by exon 10 of *RB1*. In Western blot analyses, this antibody recognizes both phosphorylated and

underphosphorylated forms of the RB1 protein. Staining can be completely blocked by an excess of the immunizing peptide. For immunohistochemical staining, frozen sections stored at −70°C were defrosted for 30 min at room temperature and fixed in cold methanol:acetone (1:1 volume) at 4°C for 10 min. After being rinsed three times in PBS, they were incubated for 15 min with 0.1% H_2O_2 in PBS, followed by 15 min incubation with avidin-blocking solution and 15 min incubation with biotin-blocking solution (Vector Laboratories Inc., Burlingame, CA, USA). The sections were then blocked with 10% goat serum in 2% BSA–PBS for 30 min and incubated overnight at 4°C with RB-WL-1 polyclonal anti-RB1 antibody at 0.25 μg/ml in 2% BSA–PBS. The bound antibody was visualized by avidin–biotin complex assay using a VECTASTAIN ABC Kit (Vector Laboratories Inc., Burlingame, CA, USA) with 3,3′-diaminobenzidine as a chromogen. The sections were washed, counterstained with hematoxylin, dehydrated, and mounted. The immunohistochemical staining for RB1 protein was performed on all mucosal samples of the eight cystectomies and on additional 14 bladder tumor samples. HGIN and TCC lesions were considered to be RB1 negative only if the cells showed no RB1 nuclear staining and contiguous RB1-positive normal cells were present as an internal positive control. Sections of human TCC with a known sequence status (wild type and mutant) of *RB1* were included as positive and negative controls in each run. Additional negative controls consisted of sections in which the positive nuclear stain with RB-WL-1 antibody was blocked by an excess of the immunizing peptide. To rule out nonspecific binding of the detection system components, sections with known positive staining for *RB1* gene were processed without incubation with RB-WL-1. The RB1 protein status was finally superimposed over the histologic map and compared with the distribution patterns of *RB1* sequencing data as well as losses within the 13q14 region.

Methylation-Specific PCR for *RB1* promoter region

To rule out the possibility of loss of RB1 protein expression due to methylation of the RB1 CpG island, a methylation-specific PCR (MPS) was performed on DNA corresponding to invasive TCC from eight cystectomy specimens. The methylation-specific PCR for *RB1* CpG island was designed and carried out as described previously.[24,25] Briefly, 1 μg of DNA was denatured by incubation with 0.2 M NaOH for 15 min at 37°C. Aliquots of 10 mM hydroquinone (30 μl) (Sigma Chemical Co., St Louis, MO, USA) and 3 M sodium bisulfite (pH 5.0, 520 μl) (Sigma Chemical Co.) were added, and the solution was incubated at 52°C for 16 h. Treated DNA was purified by use of a Wizard DNA Purification System (Promega Corp., Madison, WI, USA). Modified DNA was stored at −80°C until used. Treatment of genomic DNA with sodium bisulfite-converts unmethylated cytosines (but not methylated cytosines) to uracil, which are then converted to thymidine during subsequent PCR.[24] Thus, after bisulfite treatment, alleles that were originally methylated have DNA sequences different from those of their corresponding unmethylated alleles, and these differences can be used to design PCR primers that are specific for methylated or unmethylated alleles. Unmethylated primers for *p16* were

Figure 1 Assembly of whole-organ histologic and genetic maps. (**a**) A gross photograph of an open cystectomy specimen with an invasive carcinoma (an area indicated by a white line) (upper panel) (map 5). The histologic map of the entire organ was generated by dividing the mucosa into 1 × 2 cm rectangular samples, which were evaluated microscopically on frozen sections stained with hematoxylin and eosin. The results of microscopic evaluation of individual samples were recorded as a histologic map (lower panel). The histologic map code is as follows: NU, normal urothelium; MD, mild dysplasia; MdD, moderate dysplasia; SD, severe dysplasia; CIS, carcinoma *in situ*; and TCC, invasive transitional cell carcinoma. An example of the relationship between allelic loss for three markers (RB1.2, RB1.20, and D13S268) and the development of precancerous *in situ* conditions is shown. The positions of these markers on the sex-averaged recombination-based map of chromosome 13 as well as their band positions are shown on the left. The areas that were involved by clonal allelic losses of markers were superimposed over the histologic map and are delineated by continuous, interrupted, and dotted lines. The markers RB1.2, RB1.20, and D13S268 show overlapping plaque-like clonal LOH involving almost the entire mucosa. (**b**) Representative microscopic samples of NU, precursor *in situ* conditions, preneoplastic lesions, and TCC are shown. For the statistical analysis, intraurothelial precursor conditions were classified into two groups: low-grade intraurothelial neoplasia (LGIN, mild to moderate dysplasia) and high-grade intraurothelial neoplasia (HGIN, severe dysplasia and carcinoma *in situ*). (**c**) Examples of clonal LOH involving almost the entire bladder mucosa for the marker RB1.20 located within intron 20 of *RB1* and marker D13S268 located approximately 3 Mb telomerically from *RB1* in the same cystectomy specimen as shown in (**a**) are illustrated (map 5). In addition, a marker D13S268 with retention of heterozygosity in all mucosal samples from map 4 is shown. Finally, marker D13S217 with LOH involving the smaller allele in areas of bladder mucosa corresponding to HGIN and TCC from map 5 is shown. Sample #1 shows the allelic pattern of the marker from peripheral blood lymphocytes (PBDNA) from the same patient and is used as a control. The presence of allelic imbalance indicative of LOH was confirmed by densitometry and is provided as the OD ratio below each sample. OD ≤ 0.5 was considered indicative of LOH. (**d–f**) Examples of allelic losses based on testing of all 40 markers on chromosome 13 identified in map 4 (**d**), map 5 (**e**), and map 6 (**f**) are shown. The vertical axes represent recombination-based maps of chromosome 13 with positions of markers and their chromosomal locations. Only markers with allelic loss are shown. The shaded blocks represent areas of urinary bladder mucosa with LOH as they relate to progression of neoplasia as shown in a histologic map of cystectomy depicted at the bottom of each diagram. Note that several markers show clonal LOH in the form of plaques involving large areas of urinary bladder mucosa. Although each specimen shows a distinct pattern of losses, markers mapping to 13q14 region that contain *RB1* consistently exhibited clonal allelic losses in the form of overlapping plaques involving large areas of bladder mucosa. Such a pattern of losses indicates that they were involved in early incipient phases of bladder neoplasia associated with clonal *in situ* expansion antecedent to the development of microscopically recognizable precursor conditions such as dysplasia. More important markers mapping to flanking regions of *RB1* were at times asynchronous with losses of markers located within *RB1* (see map 4 shown in (**d**).

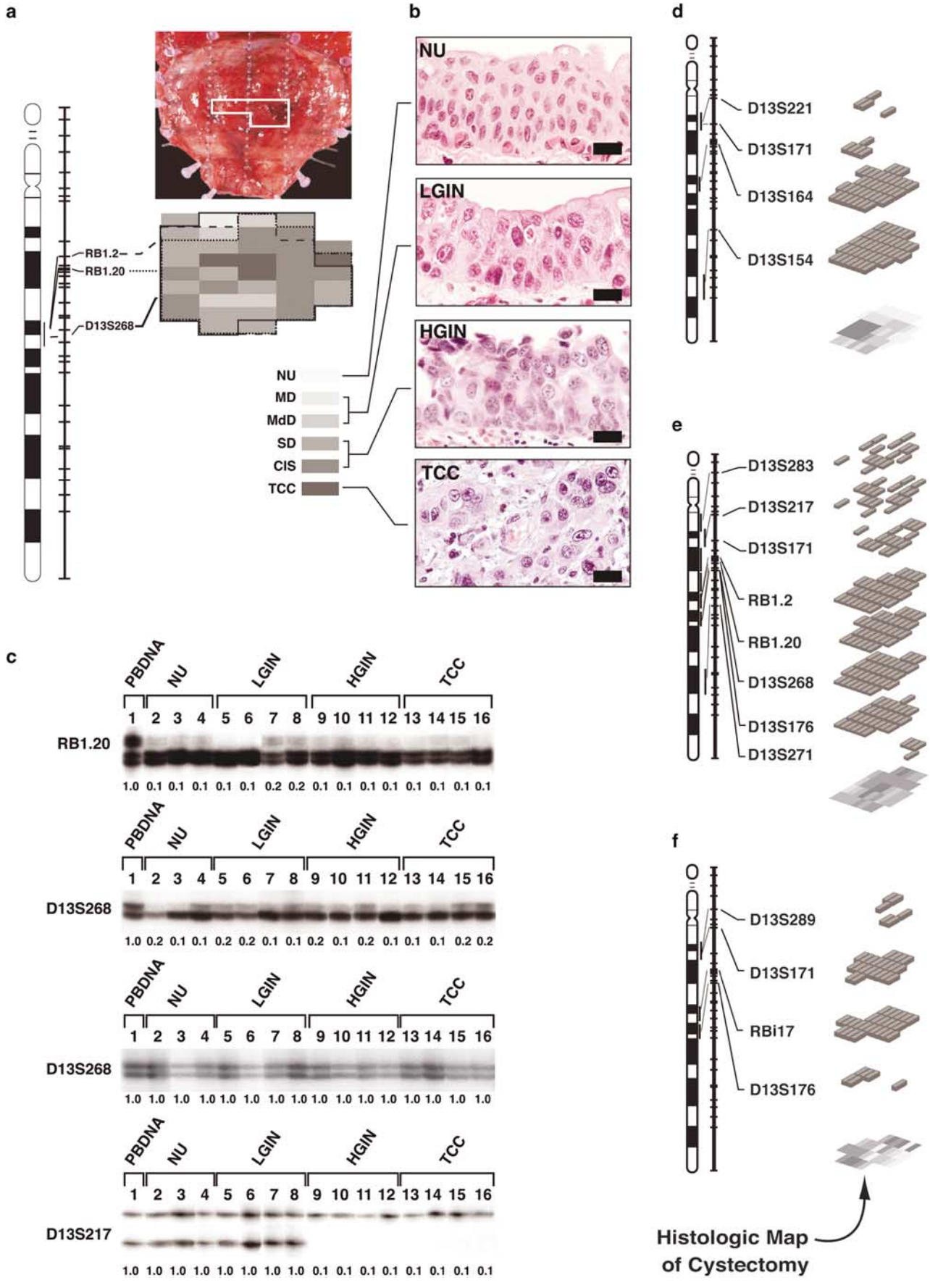
a
RB1.2
RB1.20
D13S268
b
NU
LGIN
HGIN
TCC
NU
MD
MdD
SD
CIS
TCC
c
PBDNA
NU
LGIN
HGIN
TCC
1 2 3 4 5 6 7 8 9 10 11 12 13 14 15 16
RB1.20
1.0 0.1 0.1 0.1 0.1 0.1 0.2 0.2 0.1 0.1 0.1 0.1 0.1 0.1 0.1 0.1
D13S268
1.0 0.2 0.1 0.1 0.2 0.2 0.1 0.1 0.2 0.1 0.2 0.1 0.1 0.1 0.2 0.2
D13S268
1.0 1.0 1.0 1.0 1.0 1.0 1.0 1.0 1.0 1.0 1.0 1.0 1.0 1.0 1.0 1.0
D13S217
1.0 1.0 1.0 1.0 1.0 1.0 1.0 1.0 0.1 0.1 0.1 0.1 0.1 0.1 0.1 0.1
d
D13S221
D13S171
D13S164
D13S154
e
D13S283
D13S217
D13S171
RB1.2
RB1.20
D13S268
D13S176
D13S271
f
D13S289
D13S171
RBi17
D13S176
Histologic Map
of Cystectomy

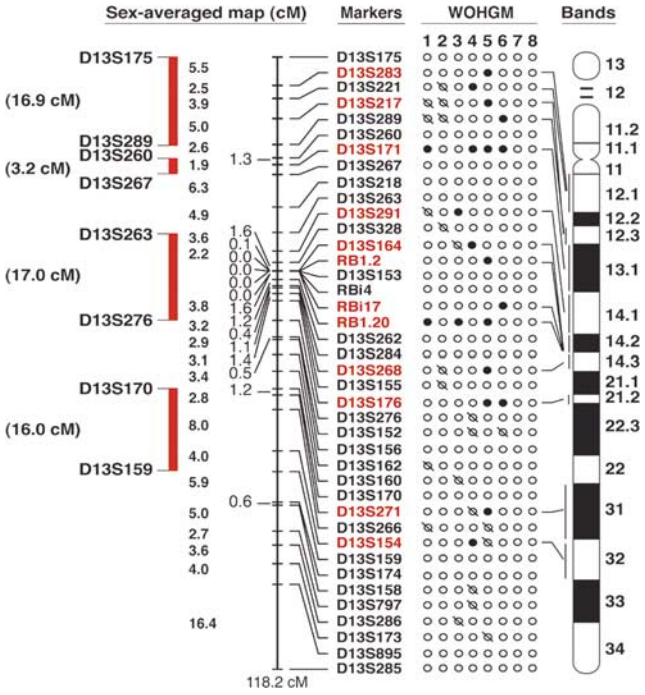

Figure 2 Deletion map of chromosome 13 assembled from data generated by whole-organ histologic and genetic mapping. A list of all tested markers and their positions according to the updated Cooperative Human Linkage Center Map is shown. Chromosomal band locations are provided for markers with LOH only. Markers printed in red showed statistically significant relationship between LOH and the development of urothelial neoplasia tested by binomial maximum-likelihood analyses and calculated as LOD scores. Red bars on the left side of the map identify the deleted regions, which are defined by the positions of deleted markers and their nearest flanking markers with retention of heterozygosity and the predicted size of the deleted regions in centimorgans (cM, centimorgans; WOHGM, whole-organ histologic and genetic mapping of individual cystectomy specimens consecutively numbered 1–8. ○, markers with retention of heterozygosity; ●, markers with LOH, and Ø, noninformative marker).

used to confirm the integrity of tissue-extracted bisulfite treated DNA.[25] DNA from peripheral blood lymphocytes of healthy volunteers were used as negative controls for MSP assays. The DNA samples from peripheral blood lymphocytes treated with *Sss*I methyltransferase (New England Biolabs, Beverly, MA, USA) and subjected to bisulfite treatment was used as a positive control for methylated alleles. Water blanks and PCR cocktails (without template) were used as negative controls in each assay. PCR products were visualized on 2% agarose gels stained with ethidium bromide.

Analysis of Data

The patterns of allelic losses identified by the microsatellite SNP markers and their relationship to the development of bladder neoplasia were analyzed by nearest-neighbor and binomial maximum-likelihood algorithms as described previously.[6–11] For statistical analyses, the whole-organ histologic and genetic mapping data were organized in a 2×4 contingency tables (f_{ji}, $j=1,\ 2;\ i=1,\ldots,4$). The columns designated whether the marker retained or lost heterozygosity and the four grades represented the microscopic status of the urothelium (D_0 normal urothelium (NU), D_1 low-grade intraurothelial neoplasia, D_2 high-grade intraurothelial neoplasia, and D_3, TCC).

A nearest-neighbor analysis was performed on the three-dimensional stacks of maps consisting of plots of marker alterations by location on the histologic bladder maps and on chromosomal vectors. An altered region was considered a neighbor of another altered region if the two were side by side in the same marker plot above and below each other. An altered region was also considered to be connected to another altered region if there was a continuous string of altered regions between them. Since the bladder was laid open and pinned flat, the left- and right-most regions were also neighbors.

The binomial maximum-likelihood analysis was performed in the same 2×4 contingency tables. The maximum likelihood of the binomial distribution was calculated for each urothelial status (D_i, $i=0,\ldots,3$) corresponding to NU, LGIN, HGIN, and TCC. The maximum likelihood for the binomial distribution was used to determine whether a row of data was consistent with a hypothesis of an unchanged (all negative) marker by calculating the log likelihood with

$$l_i = \ln\left(\frac{\theta_i^{f_{1i}}(1-\theta_i)^{f_{2i}}}{\hat{\theta}_i^{f_{1i}}(1-\hat{\theta}_i)^{f_{2i}}}\right)$$

Figure 3 Summary of physical map and sequence database analysis spanning the deleted regions of chromosome 13. The Genethon positions of the markers defining the deleted regions were related to the GB4 radiation hybrid panel-based physical map. The new positions for the Genethon markers with LOH as well as flanking markers on the GB4 map were identified by electronic PCR search of BAC contigs. In addition, multiple alternative markers based on their proximity to markers with LOH were identified and added to the map. The nearest substitute markers are often located within the same BAC clone as original Genethon markers used for LOH studies. Consequently, some of the original Genethon and substitute markers have the same position on the GB4 map. The original Genethon markers with LOH are shown in red, while all other substitute and flanking markers are printed in black. An average EST density is provided for regions flanked by individual markers using the GB4 radiation panel map. The list of known genes within the target regions and their positions on the GB4 map is shown. In the final steps, we extracted all known, proposed, and predicted genes between markers using the sequence-based mapping tools at the Ensemble website and the 'Golden Path' Genome Browser and constructed final sequence-based map of the deleted chromosomal regions putatively involved in progression of bladder neoplasia from precursor conditions to invasive cancer. To simplify the diagram, only the first position of a gene sequence on the GB4 map is shown. More complete data with contigs information and alternative positions of the genes as well as the addresses for gene sequences can be obtained from http://www.mdanderson.org/BladderGenomicMaps.

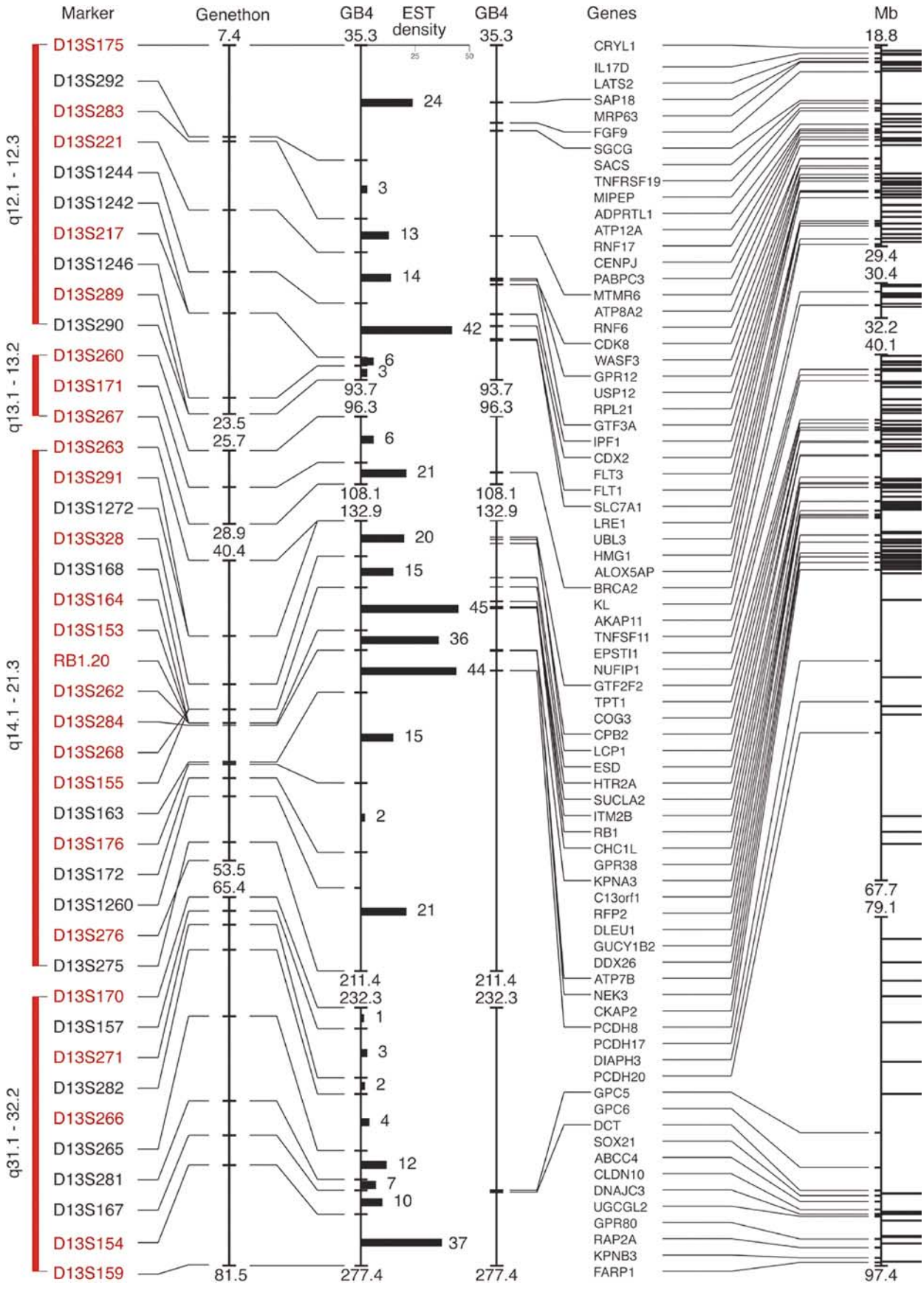
Marker
Genethon
GB4
EST density
GB4
Genes
Mb
q12.1 - 12.3
q13.1 - 13.2
q14.1 - 21.3
q31.1 - 32.2
D13S175
D13S292
D13S283
D13S221
D13S1244
D13S1242
D13S217
D13S1246
D13S289
D13S290
D13S260
D13S171
D13S267
D13S263
D13S291
D13S1272
D13S328
D13S168
D13S164
D13S153
RB1.20
D13S262
D13S284
D13S268
D13S155
D13S163
D13S176
D13S172
D13S1260
D13S276
D13S275
D13S170
D13S157
D13S271
D13S282
D13S266
D13S265
D13S281
D13S167
D13S154
D13S159
7.4
23.5
25.7
28.9
40.4
53.5
65.4
81.5
35.3
93.7
96.3
108.1
132.9
211.4
232.3
277.4
24
3
13
14
42
6
3
6
21
20
15
45
36
44
15
2
21
1
3
2
4
12
7
10
37
CRYL1
IL17D
LATS2
SAP18
MRP63
FGF9
SGCG
SACS
TNFRSF19
MIPEP
ADPRTL1
ATP12A
RNF17
CENPJ
PABPC3
MTMR6
ATP8A2
RNF6
CDK8
WASF3
GPR12
USP12
RPL21
GTF3A
IPF1
CDX2
FLT3
FLT1
SLC7A1
LRE1
UBL3
HMG1
ALOX5AP
BRCA2
KL
AKAP11
TNFSF11
EPSTI1
NUFIP1
GTF2F2
TPT1
COG3
CPB2
LCP1
ESD
HTR2A
SUCLA2
ITM2B
RB1
CHC1L
GPR38
KPNA3
C13orf1
RFP2
DLEU1
GUCY1B2
DDX26
ATP7B
NEK3
CKAP2
PCDH8
PCDH17
DIAPH3
PCDH20
GPC5
GPC6
DCT
SOX21
ABCC4
CLDN10
DNAJC3
UGCGL2
GPR80
RAP2A
KPNB3
FARP1
18.8
29.4
30.4
32.2
40.1
67.7
79.1
97.4

for the null hypothesis H_0, where $\theta = \theta_i$ and $\theta = f_{1i}/(f_{1i}+f_{2i})$ is the maximum-likelihood estimate of a negative marker. Two times the negative of the log likelihood, $-2l_i$, is asymptotically χ^2 with 1 df, $\chi^2(1)$. This expression can be written as

$$-2l_i = 2\ \ln(10)\log_{10}\left(\frac{\hat{\theta}_i^{f_{1i}}(1-\hat{\theta}_i)^{f_{2i}}}{\theta_i^{f_{1i}}(1-\theta_i)^{f_{2i}}}\right)$$
$$= 2\ \ln(10)\mathrm{LOD}(\hat{\theta}_i : \theta_i)$$

where $\mathrm{LOD}(\hat{\theta}_i{:}\theta_i)$ is the LOD-score function evaluated at θ_i.[26] Each row of the table for which $-2l_i$ have approximate $\chi^2(1)$ can be tested separately (stringency level 1) or all rows for diagnosis D_i and more advanced $(D_i, \ldots, D3)$ can be combined (stringency level 2) to get

$$f_{1i+} = \sum_{j=i}^{3} f_{1j}$$

$$f_{2i+} = \sum_{j=i}^{3} f_{2j}$$

$$\mathrm{LOD}(\hat{\theta}_{i+} : \theta_{i+}) = \log_{10}\left(\frac{\hat{\theta}_{i+}^{f_{1i+}}(1-\hat{\theta}_{i+})^{f_{2i+}}}{\theta_i^{f_{1i+}}(1-\theta_{i+})^{f_{2i+}}}\right),$$

which is also $\chi^2(1)$ after adjustment by $2\ln(10) = 4.605$. As the maximum-likelihood estimates for the individual rows are usually different from each other, the sum of the LOD scores and the sum of the χ^2 were greater than the combined statistics.

A χ^2 test for heterogeneity was appropriate to test the combined estimate.[26] Usually, $\theta_i = 0.5$ is used to test linkage in familial disorders with meiotic segregation of the phenotype.[27] With reference to sporadic cancer and especially when populations of tested cells represent sequential stages of the process with mitotic transmission of the phenotype, the null hypothesis is more appropriately verified at θ differing from 0.5. For example, a value of 0.99 is more appropriate if the marker is unchanged in the tissue, and a value of 0.01 is more appropriate for determining whether the marker has been altered from an unchanged to a changed state in the later stages of the process, that is, invasive carcinoma. The pattern of LOD scores ≥ 3 at $\theta = 0.01$ or 0.99 and LOD scores < 3 at $\theta = 0.5$ for the same marker is significant. The strongest association between an altered marker and neoplasia is when an LOD score is ≥ 3 at $\theta = 0.99$ and 0.5 and < 3 at $\theta = 0.01$. It has to be understood that the use of LOD in linkage analysis of familial genetic predisposition for diseases is intended to be used in its generic mathematical sense as likelihood tests of events. We used the LOD score variant of the likelihood test as many researchers are more familiar with approximate levels of significance when expressed in this form.

The analysis of the relationship among LOH in individual loci and various clinicopathological parameters of tumors and of voided urine samples was tested by Gehan's generalized Wilcoxon and log-rank tests ($P \leq 0.05$ was considered significant).

Results

Recombination-Based Deletion Map of Chromosome 13

We searched for allelic losses using the 40 hypervariable DNA markers mapping to chromosome 13. Our initial analysis of paired normal and tumor DNA samples identified LOH in five of eight cystectomy specimens and they involved 14 of 40 tested markers. Markers with LOH were subsequently tested on all mucosal samples, and their losses were related to the geographic distribution of intraurothelial neoplastic lesions and invasive cancer (Figure 1a–f). Four clusters of allelic losses mapped to distinct regions of chromosome 13 were identified (Figure 2). The deleted regions defined by the nearest flanking markers with retention of heterozygosity and their predicted size in centimorgan (cM) were as follows: 13q12 (D13S175–D13S289, 16.9 cM), 13q13 (D13S260–D13S267, 3.2 cM), 13q14 (D13S263–D13S276, 17.0 cM), 13q31 (D13S170–D13S159, 16.0 cM).

The segment flanked by D13S263 and D13S276, which contains *RB1*, showed clonal allelic losses in five of eight tested bladders. Clonal allelic losses in this region involved large areas of bladder mucosa encompassing not only invasive cancer and adjacent severe dysplasia or carcinoma *in situ* but also areas of low to moderate dysplasia focally extending to areas of microscopically NU. Clonal losses of individual markers mapping to this region formed closely overlapping plaques over a large area of bladder mucosa, suggesting that such losses are associated with the *in situ* expansion and establishment of a dominant preneoplastic clone (Figure 1a–f). More importantly, losses of markers located around

Figure 4 Summary of data on allelic losses using markers mapping to deleted regions of chromosome 13 tested in 25 bladder tumors and 21 voided urine samples. (**a**) A list of alterations in individual bladder tumor tissues and voided urine samples is provided. The losses are related to clinicopathologic parameters such as growth pattern, histologic grade, and stage of tumor. Markers located within *RB1* are designated by a shaded area. Markers mapping to centromeric (Cent) and telomeric (Tel) regions flanking *RB1* are designated by the brackets at the bottom of the figure. The immunohistochemical results of RB protein expression (RB1(IH)) in 14 tumor samples are summarized in the boxed column on the right. The bladder tumor and voided urine samples listed are not from the same patients. (**b**) Frequency of allelic loss in four deleted regions on chromosome 13 is shown. Loss in the 13q14 *RB1*-containing region can be detected in 32 and 38% of bladder tumors and voided urine samples, respectively. (**c**) Frequency of allelic loss in centromeric-(Cent) and telomeric-(Tel) flanking regions and within *RB1* is illustrated.

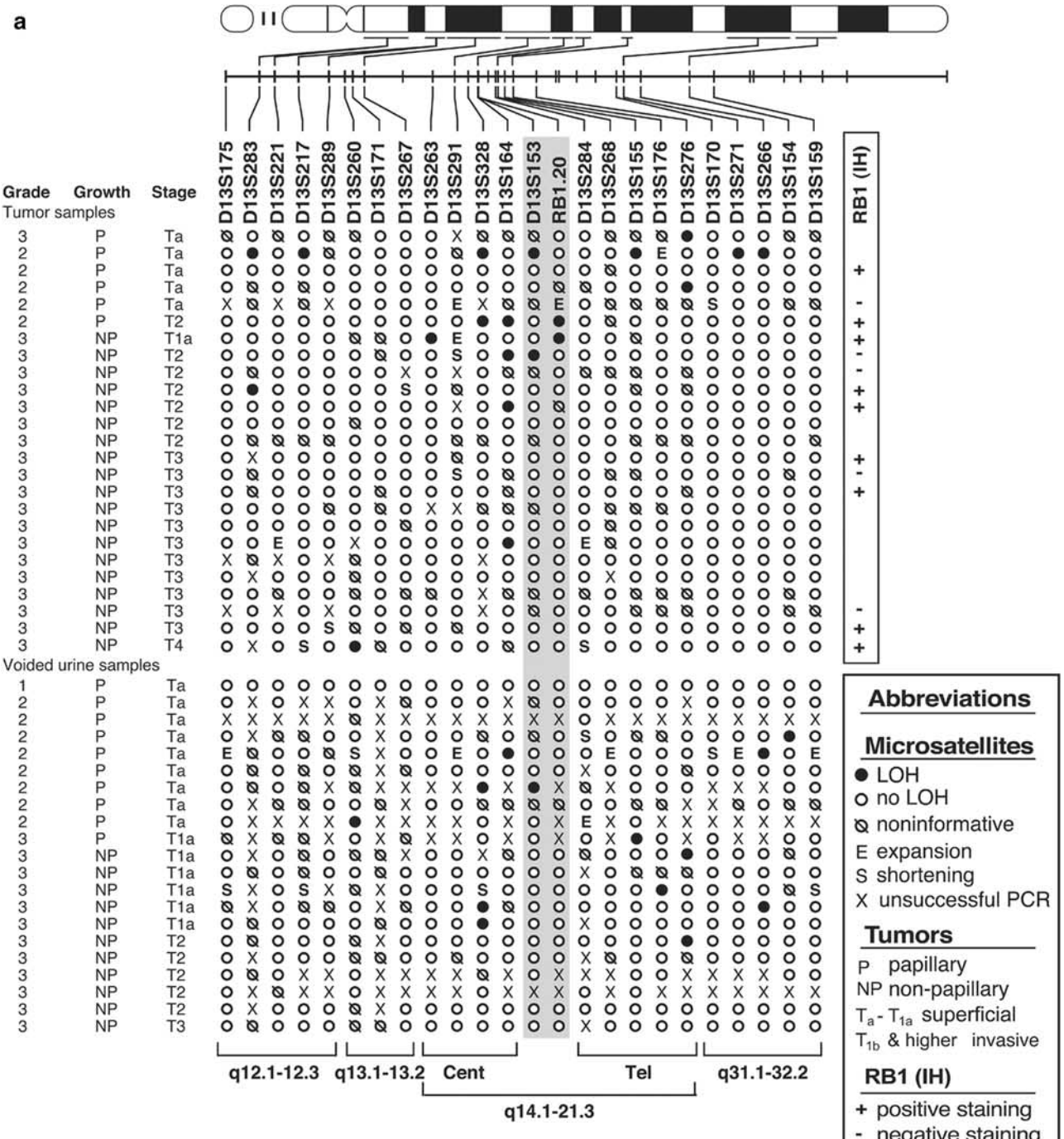
a
Grade Growth Stage
Tumor samples
3 P Ta
2 P Ta
2 P Ta
2 P Ta
2 P Ta
2 P T2
3 NP T1a
3 NP T2
3 NP T2
3 NP T2
3 NP T2
3 NP T2
3 NP T2
3 NP T3
3 NP T3
3 NP T3
3 NP T3
3 NP T3
3 NP T3
3 NP T3
3 NP T3
3 NP T3
3 NP T3
3 NP T4
Voided urine samples
1 P Ta
2 P Ta
2 P Ta
2 P Ta
2 P Ta
2 P Ta
2 P Ta
2 P Ta
2 P Ta
3 P T1a
3 NP T1a
3 NP T1a
3 NP T1a
3 NP T1a
3 NP T1a
3 NP T2
3 NP T2
3 NP T2
3 NP T2
3 NP T2
3 NP T3
D13S175
D13S283
D13S221
D13S217
D13S289
D13S260
D13S171
D13S267
D13S263
D13S291
D13S328
D13S164
D13S153
RB1.20
D13S284
D13S268
D13S155
D13S176
D13S276
D13S170
D13S271
D13S266
D13S154
D13S159
RB1 (IH)
q12.1-12.3
q13.1-13.2
Cent
Tel
q31.1-32.2
q14.1-21.3
Abbreviations
Microsatellites
LOH
no LOH
noninformative
E expansion
S shortening
X unsuccessful PCR
Tumors
P papillary
NP non-papillary
Ta - T1a superficial
T1b & higher invasive
RB1 (IH)
+ positive staining
- negative staining
b
Tumor (P<0.001)
Urine (P<0.001)
Frequency %
q12.1-12.3
q13.1-13.2
q14.1-21.3
q31.1-32.2
Deleted regions
c
Tumor (P=0.52)
Urine (P=0.31)
Frequency %
Cent
RB1
Tel
Deleted regions

RB1 were at times asynchronous with a loss of markers located within *RB1* (Figure 1d–f). The allelic losses of the three remaining segments mapping to 13q12, 13q13, and 13q31 exhibited a limited relationship to clonal expansion of intraurothelial neoplastic lesions, suggesting they do not necessarily progress to invasive carcinoma.

Integration of Recombination-Based Deletion Map with Genome Sequence Database

The deleted regions of chromosome 13 defined by hypervariable DNA markers were integrated with the physical map and ultimately with the human genome sequence (Figure 3). Using this approach, we were able to identify all known and predicted genes mapping to the regions involved in bladder neoplasia. Besides the model tumor suppressor gene, *RB1*, 29 known and 71 predicted genes, some of which were putative tumor suppressor genes, were identified in the most frequently deleted region mapping to 13q14. Other less frequently deleted regions of chromosome 13 also contained genes with well-established tumor suppressor functions such as *BRCA2*, which maps to 13q13 region. In addition, all deleted regions on chromosome 13 involved in bladder neoplasia contained several genes involved in cell cycle regulation or coded for proteins regulating cell differentiation and cell–stroma interactions.

Testing of Tumors and Urine Samples

Since the major limitation of whole-organ histologic and genetic mapping studies is that they can only be performed on a limited number of cases, we have tested the markers located within the deleted regions on chromosome 13 on a larger number of tumor and voided urine samples from patients with bladder cancer (Figure 4a). This approach revealed that allelic loss of markers mapping to the 13q14 RB1-containing segment could be detected in approximately 32 and 38% of bladder tumor tissues and urine samples of patients with bladder cancer, respectively (Figure 4b). Allelic losses in the three remaining deleted regions could be detected in less than 15% of tumors (Table 1). It is therefore highly unlikely that they contained tumor suppressor genes frequently involved in the development of bladder cancer. Interestingly, allelic loss within 13q14 was seen more frequently in superficial bladder tumors than in invasive carcinomas, but could not be related to histologic grade or growth pattern (Table 1). More importantly, such loss did not necessarily correlate with the inactivation of *RB1* gene as documented by immunohistochemical staining of tumor tissues (Figure 4a). In addition, although statistically nonsignificant, markers mapping to flanking regions of *RB1* exhibited LOH more often than markers located within *RB1*.

Table 1 Frequency of LOH in four regions of chromosome 13 in bladder TCC and voided urine samples

	13q12 (D13S175–D13S289)			*13q13 (D13S260–D13S267)*			*13q14 (D13S263–D13S276)*			*13q31 (D13S170–D13S159)*		
	Frequency (%)		P-*value*	*Frequency (%)*		P-*value*	*Frequency (%)*		P-*value*	*Frequency (%)*		P-*value*
	Tumor	*Urine*	*Tumor* *Urine*	*Tumor*	*Urine*	*Tumor* *Urine*	*Tumor*	*Urine*	*Tumor* *Urine*	*Tumor*	*Urine*	*Tumor* *Urine*
Growth pattern												
Papillary	16.7 (1/6)[a]	0	0.43 —	0	10.0 (1/10)	0.57 0.48	66.7 (4/6)	30.0 (3/10)	0.37 0.66	16.7 (1/6)	20.0 (2/10)	0.07 0.59
Nonpapillary	5.3 (1/19)	0		5.3 (1/19)	0		21.1 (4/19)	45.5 (5/11)		0	9.1 (1/11)	
Histologic grade												
Low grade (1–2)	33.3 (1/3)	0	0.23 —	0	11.1 (1/9)	— 0.43	66.7 (2/3)	22.2 (2/9)	0.23 0.37	33.3 (1/3)	22.2 (2/9)	0.12 0.55
High grade (3)	4.5 (1/22)	0		4.5 (1/22)	0		27.3 (6/22)	50.0 (6/12)		0	8.3 (1/12)	
Stage												
Superficial (T_a–T_{1a})	16.7 (1/6)	0	0.43 —	0	6.7 (1/15)	— —	66.7 (4/6)	46.7 (7/15)	0.04 0.34	16.7 (1/6)	20.0 (3/15)	0.24 0.53
Invasive (T_{1b}–T_4)	5.3 (1/19)	0		5.3 (1/19)	0		21.1 (4/19)	16.7 (1/6)		0	0	
Total	8	0		4	4.8		32	38.1		4	14.3	

[a]Numbers within parenthesis indicate number of cases with LOH *vs* number of informative cases with retention of heterozygosity within the group.

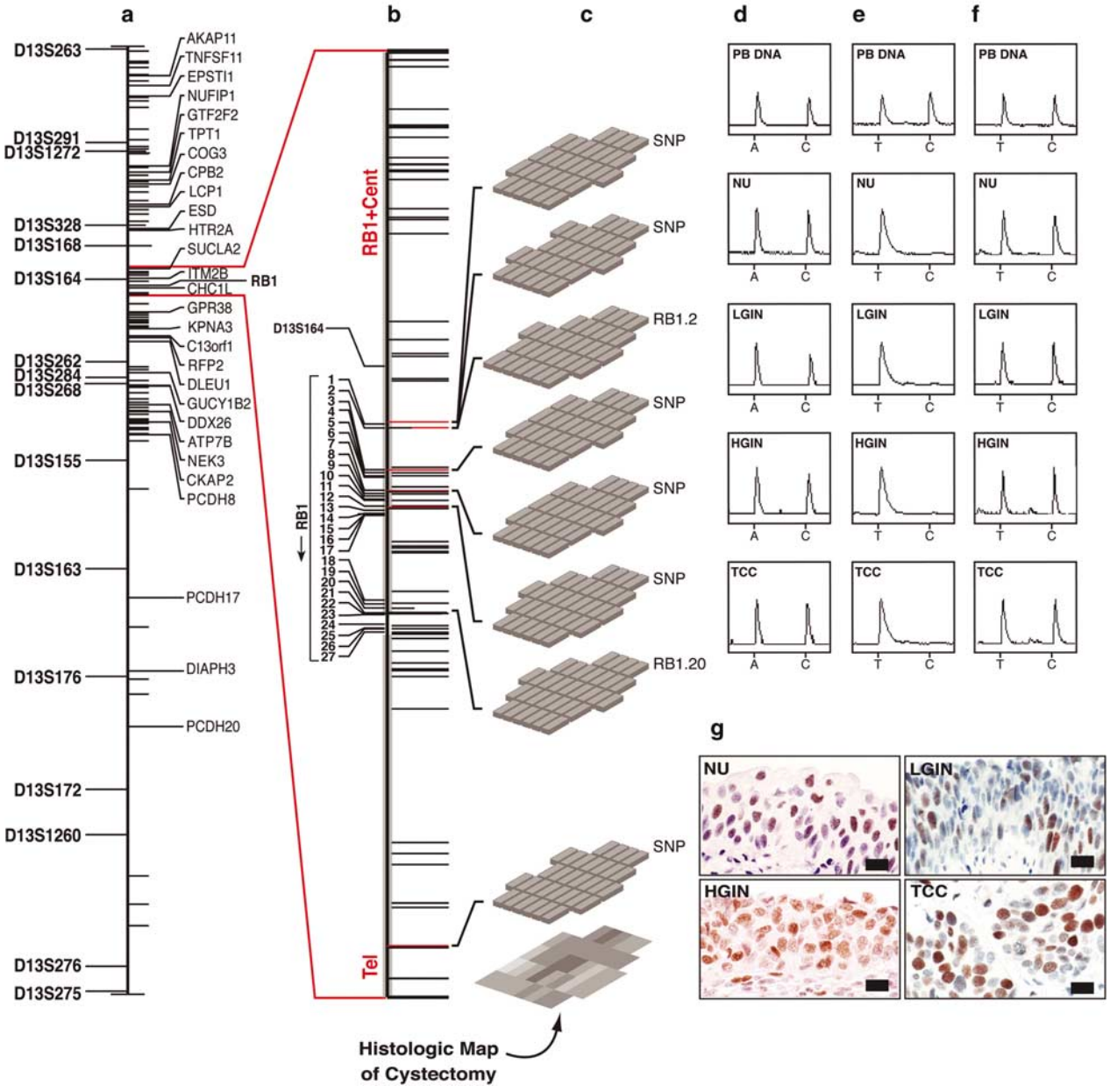

Figure 5 An example of high-resolution whole-organ mapping by genotyping of SNPs and the assembly of LOH distribution patterns in a single cystectomy specimen. (**a**) A sequence-based map of a 27-Mb region flanked by markers D13S263 and D13S275 is shown. The positions of hypervariable markers are shown on the left side of the map. Bars on the right side of the map depict the positions of known and predicted genes. (**b**) The genomic map of *RB1*, *ITM2B*, and *CHC1L* with its flanking regions spanning 0.8 Mb is expanded. The positions of the *RB1*, *ITM2B*, and *CHC1L* exons are shown on the left side of the map. The positions of 79 SNPs and hypervariable DNA markers are shown on the right side of the map. The arrow in the expanded map indicate the direction of transcription for *RB1*. (**c**) The distribution of clonal allelic losses as they relate to preneoplastic *in situ* lesions and invasive carcinoma shown as a histologic map at the bottom is illustrated (map 5). The blocks illustrate the distribution of clonal allelic losses identified by SNPs and RB1.2 as well as RB1.20 markers. The code for the histologic map is identical to the code shown in Figure 1. A clonal plaque-like loss involving a large area of bladder mucosa for the markers and SNPs within *RB1* and its flanking centromeric (Cent) and telomeric (Tel) region is evident. The predicted size of lost regions estimated by the positions of hypervariable DNA markers and SNP with loss of polymorphism and the positions of nearest-flanking markers with retention of heterozygosity or SNPs with retention of polymorphism is depicted by the shaded vertical bars superimposed over the map. (**d**) An example of retention of an A/C polymorphism in all bladder mucosal samples of the first informative SNP above *ITM2B*, which defines the upper centromeric border of the deleted region is shown. (**e**) An example of clonal loss of a T/C polymorphism in SNP located within *RB1*. Note that peripheral blood sample of the same patient shows retention of a T/C polymorphism in the same SNP. (**f**) An example of retention of a T/C polymorphism in all mucosal samples of the first informative SNP located below *RB1*, which defines the telomeric border of the allelic loss involving *RB1* and its proximal–centromeric region. It also defines a breakpoint between a separate region of allelic loss located telomerically to *RB1*. (**g**) The presence of RB1 protein expression corresponding to NU, LGIN, HGIN, and TCC correlated with the sequencing data, which documented that the wild-type sequence of the remaining *RB1* allele was retained in this case. Positive RB1 nuclear staining was seen in samples corresponding to preneoplastic *in situ* lesions (LGIN and HGIN) as well as in TCC. Solid black bars, 50 μm.

This trend was particularly evident when allelic losses within *RB1* and its flanking regions were tested on voided urine samples of patients with bladder cancer (Figure 4c). Overall these data provided evidence that the 13q14 region of chromosome 13 is most frequently altered in bladder neoplasia and confirmed whole-organ histologic and genetic mapping data supporting the concept of alternative target genes mapping to flanking regions of *RB1*.

Integration of SNP-Based Deletion Map of *RB1* with *RB1* Sequencing, Promoter Methylation, and RB1 Protein Expression Status

We next focused our attention on the pattern of *RB1* involvement in the development of urothelial neoplasia by genotyping SNP sites within and around *RB1* in all mucosal samples of cystectomy specimens. When patterns of allelic losses revealed by markers mapping within and around *RB1* were integrated with *RB1* sequencing data and RB1 protein expression patterns, it became evident that losses in this region were associated with clonal expansion but not necessarily with the inactivation of the remaining *RB1* allele (Figure 5a–g). Even in those cases in which the inactivation of the remaining *RB1* allele by a point mutation took place, it was a later event that accompanied the onset of severe dysplasia/carcinoma *in situ* progressing to invasive carcinoma (Figure 6a–d). None of the cases showed an abnormal methylation pattern of the CpG island located upstream of *RB1* (Figure 6e). The pattern of alterations implied that deletions involving approximately 2 Mb segments of DNA-flanking *RB1* were important for early clonal expansion of preneoplastic lesions and that such deletions were not necessarily associated with the inactivation of the remaining *RB1* allele.

Discussion

Our observations indicate that some of the incipient events of human bladder neoplasia are associated with hits that map to flanking regions of a model tumor suppressor gene, namely *RB1*. We have provided evidence that the segment mapping to 13q14, flanked by D13S263 and D13S276, was involved in approximately 30–40% of bladder tumors and was typically lost in the early intraurothelial phases of bladder neoplasia. Moreover, the loss preceded the development of microscopically recognizable precursor lesions and did not involve loss of *RB1* function. The inactivation of *RB1* occurred later, at the time severe dysplasia/carcinoma *in situ* developed. Such a pattern of alterations in 13q14 implied that genes distinct from *RB1* but mapping to its flanking regions were involved in the expansion of the initial neoplastic clone.

Tissue culture observations show, in contrast to the findings in non-human cells, that cooperating oncogenes and tumor suppressor genes alone are not sufficient to transform normal human cells into malignant cells.[28–30] The successful creation of human tumor cells *in vitro* typically requires the use of chemical and physical agents or an entire viral genome to achieve immortalization, a prerequisite for subsequent transforming effects of cooperating oncogenes.[31–34] More recently, human epithelial and fibroblast cells were transformed *in vitro* by ectopic expression of telomerase catalytic subunit (*hTERT*) in combination with two oncogenes (the Simian virus 40 large-T oncoprotein and an oncogenic allele of *H-ras*).[35,36]

Figure 6 Integration of deletion patterns identified in the 13q14 region with *RB1* sequencing data and RB1 protein expression patterns. (**a**) The deleted regions associated with early clonal expansion identified by whole-organ histologic and genetic mapping with 79 SNPs and hypervariable DNA markers in six cystectomy specimens are related to the status of *RB1* sequence (RB1(S)) and RB1 protein expression revealed by immunohistochemistry (RB1(IH)). The results of *RB1* sequencing and protein expression are tabulated below the deletion maps of individual cystectomy specimen. The results of methylation status of *RB1* promoter region are summarized in (**e**). The blue bars in each whole-organ histologic depict the deleted regions identified by genotyping of SNPs and genetic map (WHOM) numbered 1–6. The red bars designate allelic losses identified by hypervariable DNA markers. The positions and distances of deleted regions are defined as described in Figure 5c. Maps 7 and 8 in which no allelic loss within 13q14 region was identified are not shown. Note that in map 2, losses within *RB1* and its flanking telomeric region were identified by genotyping of SNPs only. (**b**) An example of clonal allelic loss of an A/C polymorphism in SNP located below *RB1* within its flanking telomeric region (map 5). Note retention of A/C polymorphism in the peripheral blood sample (PB DNA) of the same patient. (**c**) The immunohistochemical pattern of RB1 protein expression in representative mucosal samples of map 2 (**c**). Note the absence of RB1 protein expression in HGIN and TCC corresponding to an area containing a mutant *RB1* allele. This pattern of allelic losses with and without inactivation of the remaining *RB1* allele provides evidence that other genes mapping to the flanking regions rather than *RB1* itself are involved in the initial *in situ* expansion of a preneoplastic clone (also see Figure 5). (**d**) The distribution of clonal allelic losses involving *RB1* and its flanking telomeric (Tel) region in map 2. Note that the area corresponding to the presence of mutant *RB1* and the absence of RB1 protein expression is restricted to TCC and to adjacent areas of HGIN. In contrast, an allelic loss involving the region telomeric to *RB1* is associated with clonal *in situ* expansion involving almost the entire bladder mucosa. (**e**) Summary of methylation-specific PCR in cystectomy specimens 1–8. P1, positive control—normal lymphocyte DNA (for unmethylated form) or normal lymphocyte DNA treated with *Sss*I methyl transferase (for methylated form); P2, positive control—*RB1* methylation of known retinoblastoma tumor; N, negative control is water blank or PCR cocktail without template. U, unmethylated form; and M, methylated form. *p16* was run as a control for DNA integrity. The sizes of amplified segments are shown within parentheses. Note the absence of methylation-specific product for *RB1* in tumor samples of maps 1–8, indicating that none of the cases included in the study contained *RB1* with methylated promoter. Overall, the data summarized in this figure indicate that the genes involved in clonal expansion of human bladder preneoplasia are located within approximately 2 Mb around *RB1*.

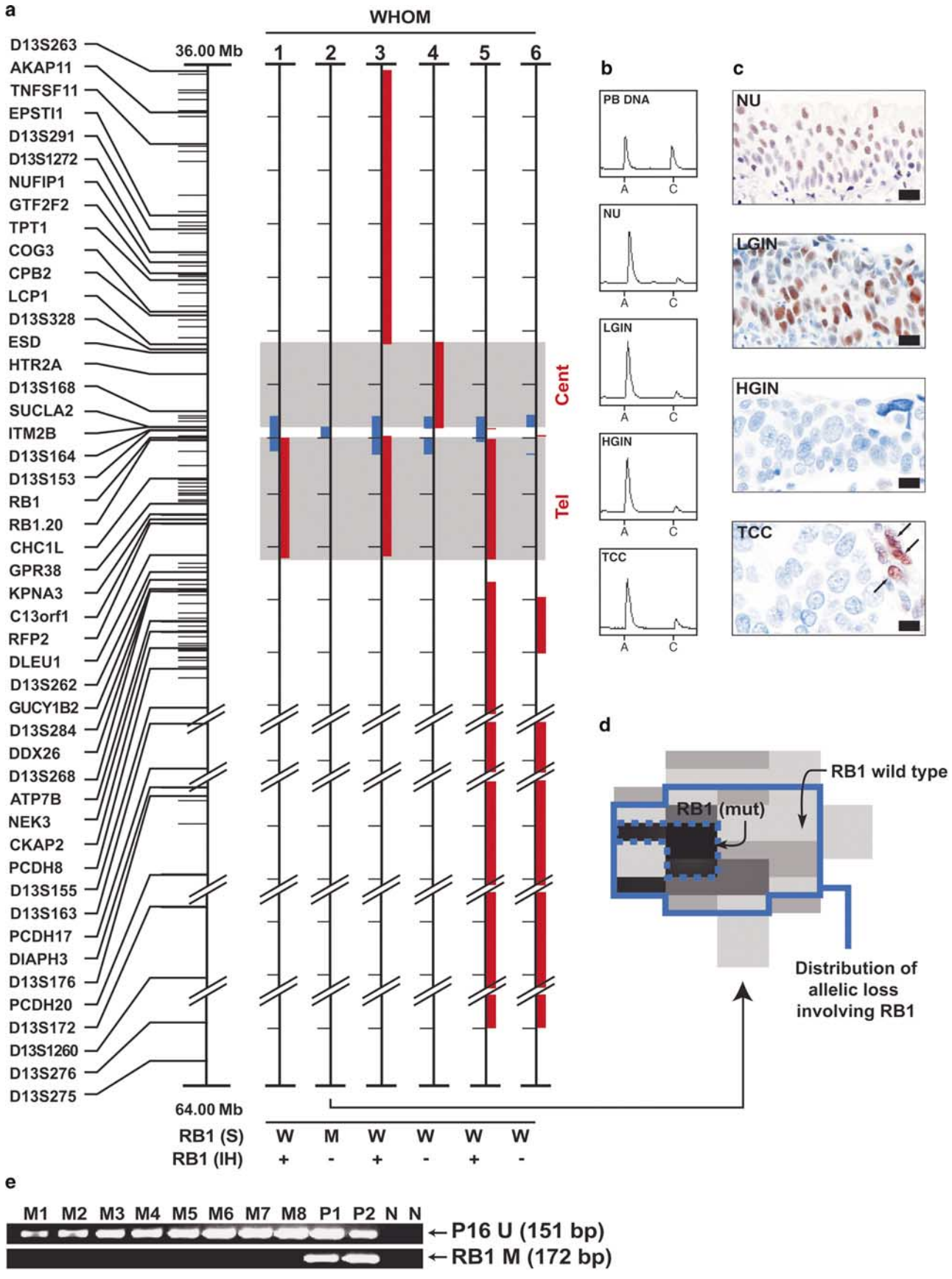
a
WHOM
D13S263
AKAP11
TNFSF11
EPSTI1
D13S291
D13S1272
NUFIP1
GTF2F2
TPT1
COG3
CPB2
LCP1
D13S328
ESD
HTR2A
D13S168
SUCLA2
ITM2B
D13S164
D13S153
RB1
RB1.20
CHC1L
GPR38
KPNA3
C13orf1
RFP2
DLEU1
D13S262
GUCY1B2
D13S284
DDX26
D13S268
ATP7B
NEK3
CKAP2
PCDH8
D13S155
D13S163
PCDH17
DIAPH3
D13S176
PCDH20
D13S172
D13S1260
D13S276
D13S275
36.00 Mb
64.00 Mb
1 2 3 4 5 6
Cent
Tel
RB1 (S) W M W W W W
RB1 (IH) + - + - + -
b
PB DNA
NU
LGIN
HGIN
TCC
A C
c
NU
LGIN
HGIN
TCC
d
RB1 wild type
RB1 (mut)
Distribution of allelic loss involving RB1
e
M1 M2 M3 M4 M5 M6 M7 M8 P1 P2 N N
← P16 U (151 bp)
← RB1 M (172 bp)

Widespread clonal *in situ* proliferations as incipient events of human neoplasia were documented *in vivo* for gastrointestinal, esophageal, and breast carcinogenesis.[1–3] Prior studies showing the discordance between allelic loss in 13q14 and the inactivation of *RB1* are in keeping with our results, and have also implicated other genes mapping to this region in the development of several human malignancies.[37–43] The presence of clonal allelic loss involving 13q14 and other regions containing tumor suppressor genes explains the efficiency of detection of bladder neoplasia by testing microsatellite markers mapping to these regions in voided urine samples.[44–46] Such markers are effective not only in detecting clinically evident bladder cancer but are also efficient tools to identify occult bladder neoplasia and predict recurrence.[47]

Whole-organ histologic maps of human bladders obtained by cystectomy, generated more than two decades ago, provided the foundation for our current pathologic concepts of urothelial neoplasia. They postulated that bladder cancer develops via two distinct but somewhat overlapping pathways, papillary and nonpapillary.[13,14] More recent molecular studies confirmed these initial clinicopathologic observations and showed that these two basic forms of bladder cancer are associated with distinct molecular alterations.[5,48,49] The involvement of major tumor suppressor genes such as *p53* and *RB1* as well as their upstream and downstream regulatory partners is typical for the high-grade nonpapillary form of bladder cancer characterized by aggressive behavior and a high propensity for distant metastasis.[5]

Our current mapping studies showed that human urothelial neoplasia starts as a widespread clonal proliferation of preneoplastic urothelial cells with the establishment of a dominant clone. In this scenario, the involvement of a key tumor suppressor gene is secondary and signifies the onset of a fully transformed phenotype with microscopic features of severe dysplasia/carcinoma *in situ* capable of progressing to invasive cancer. The possibility that the *RB1* haplotype may have an effect on the development of incipient preneoplastic conditions cannot be completely ruled out by the analysis of losses in the 13q14 region. However, the clinical data implicate that the *RB1* haplotype has no effect on cell biology as documented by the presence of familial syndromes, which carry a mutant inactive allele of *RB1* in normally developing somatic cells.[50,51] A similar alteration pattern was previously reported by us for the *p53*-containing region and provides additional support for the existence of alternative candidate genes mapping, in general, near major tumor suppressors that may be critical for the initial expansion of preneoplastic clones.[6]

The presence of clonal discontinuous deletions within the *RB1* region implies that such changes occurred during an early phase of *in situ* neoplasia. The development of such complex deletions in a form of one synchronous hit is very unlikely. The more likely scenario is that they evolved as sequential events. The presence of discontinuous deletions in the region also implies that not all of them were functionally valid and some of them were dragged through clonal expansion as passenger changes. Overall, such findings suggest that the early preclonal phase of tumor development is associated with the high degree of genetic instability followed by a more stable phase of clonal *in situ* expansion. The mapping evidence suggesting the presence of alternative positional candidate genes near *RB1* involved in the development of *in situ* neoplasia is associative, but the clonality of the hits forming large plaques in bladder mucosa and consistency of such findings suggest functional relevance. The size of the 13q14 segment involved by clonal allelic losses indicate that the alternative candidate genes should be present within approximately 2 Mb around *RB1*. The pattern of involvement of microsatellite markers mapping to the flanking regions of *RB1* tested on multiple tumor and voided urine samples, which did not reach the statistical significance, suggests that alternative positional candidate genes may, in fact, be located in close proximity to *RB1*.

The precise identification of alternative positional candidate genes near *RB1* that may drive the initial clonal expansion of bladder neoplasia will require high-throughput mapping of the 13q14 region. We estimate that for such whole-organ mapping studies, we will need allelotyping of 500–1000 SNPs in at least five informative cystectomy specimens. We predict that 10 000–15 000 tests will have to be performed to construct a precise map of sequential hits near *RB1*. Such labor intense studies are feasible with the assistance of robotic instruments and are currently being conducted in our laboratory.

Acknowledgements

This work was supported by National Institute of Health Grants UO1 CA85078 (BC), R01 CA66723 (BC), and GU SPORE Grant P50 CA91846. We would like to thank Stephanie M Rodriguez for secretarial assistance and Sandra Ideker-Soule for computerized graphical design of figures.

References

1 Carethers JM. The cellular and molecular pathogenesis of colorectal cancer. Gastroenterol Clin N Am 1996;25: 737–754.
2 Ilyas M, Straub J, Tomlinson IPM, Bodmer WF. Genetic pathways in colorectal and other cancers. Eur J Cancer 1999;35:1986–2002.
3 Watanabe T, Muto T. Colorectal carcinogenesis based on molecular biology of early colorectal cancer, with

special reference to nonpolypoid (superficial) lesions. World J Surg 2000;24:1091–1097.
4 Ayala AG, Ro JY, Amin M, *et al.* The pathology of incipient neoplasia. In: Henson DE, Albores-Saavedra J (eds). Preneoplastic Urothelial Lesions and Urothelial Malignancies. Oxford University Press: New York, 2001, pp 483–534.
5 Dinney CP, McConkey DJ, Millikan RE, *et al.* Focus on bladder cancer. Cancer Cell 2004;6:111–116.
6 Chaturvedi V, Li L, Hodges S, *et al.* Superimposed histologic and genetic mapping of chromosome 17 alterations in human urinary bladder neoplasia. Oncogene 1997;14:2059–2070.
7 Czerniak B, Chaturvedi V, Li L, *et al.* Superimposed histologic and genetic mapping of chromosome 9 in progression of human urinary bladder neoplasia: implications for a genetic model of multistep urothelial carcinogenesis and early detection of urinary bladder cancer. Oncogene 1999;18:1185–1196.
8 Czerniak B, Li L, Chaturvedi V, *et al.* Genetic modeling of human urinary bladder carcinogenesis. Genes Chromosome Cancer 2000;27:392–402.
9 Yoon D-S, Li L, Zhang RD, *et al.* Genetic mapping and DNA sequence-based analysis of deleted regions on chromosome 16 involved in progression of bladder cancer from occult preneoplastic conditions to invasive disease. Oncogene 2001;20:5005–5014.
10 Kram A, Li L, Zhang RD, *et al.* Mapping and genome sequence analysis of chromosome 5 regions involved in bladder cancer progression. Lab Invest 2001;81: 1039–1048.
11 Tuziak T, Jeong J, Majewski T, *et al.* High-resolution whole-organ mapping with SNPs and its significance to early events in carcinogenesis. Lab Invest 2005;85: 689–701.
12 Gazdar AF, Czerniak B. Filling the void: urinary markers for bladder cancer risk and diagnosis. Natl Cancer Inst 2001;93:452–454.
13 Koss LG, Tiamson EM, Robbins MA. Mapping cancerous and precancerous bladder changes. A study of the urothelium in ten surgically removed bladders. JAMA 1974;227:281–286.
14 Koss LG, Nakanishi I, Freed SZ. Nonpapillary carcinoma *in situ* and atypical hyperplasia in cancerous bladders: further studies of surgically removed bladders by mapping. Urology 1977;9:442–445.
15 Mostofi FK (ed). Histological Typing of Urinary Bladder Tumours. Springer: New York, 1999.
16 Sobin LH, Wittekind C. TNM Classification of Malignant Tumors, 5th edn. Wiley-Liss: New York, 1997.
17 Bernardini S, Billerey C, Martin M, *et al.* The predictive value of muscularis mucosae invasion and p53 over expression on progression of stage T1 bladder carcinoma. J Urol 2001;165:42–46.
18 Kim JH, Tuziak T, Hu L, *et al.* Alternations in transcription clusters underlie development of bladder cancer along papillary and nonpapillary pathways. Lab Invest 2005;85:532–549.
19 Ronaghi M, Uhlen M, Nyren P. A sequencing method based on real-time pyrophosphate. Science 1998;281: 363–365.
20 Ahmadian A, Gharizadeh B, Gustafsson AC, *et al.* Single-nucleotide polymorphism analysis by pyrosequencing. Anal Biochem 2000;280:103–110.
21 Benedict WF, Lerner SP, Zhou J, *et al.* Level of retinoblastoma protein expression correlates with p16 (MTS-1/INK4A/CDKN2) status in bladder cancer. Oncogene 1999;18:1197–1203.
22 Xu HJ, Hu SX, Hashimoto T, *et al.* The retinoblastoma susceptibility gene product: a characteristic pattern in normal cells and abnormal expression in malignant cells. Oncogene 1989;4:807–812.
23 Xu HJ, Hu SX, Benedict WF. Lack of nuclear RB protein staining in G0/middle G1 cells: correlation to changes in total RB protein level. Oncogene 1991;6: 1139–1146.
24 Herman JG, Graff JR, Myohanen S, *et al.* Methylation-specific PCR: a novel PCR assay for methylation status of CpG islands. Proc Natl Acad Sci USA 1996; 93:9821–9826.
25 Simpson DJ, Hibberts NA, McNicol AM, *et al.* Loss of pRb expression in pituitary adenomas is associated with methylation of the RB1 CpG island. Cancer Res 2000;60:1211–1216.
26 Zar Jr JH. Biostatistical Analysis, 3rd edn. Prentice-Hall: Englewood Cliffs, NJ, 1996.
27 Ott J. Analysis of Human Genetic Linkage. Johns Hopkins University Press: Baltimore, MD, 1995.
28 Sager R. Senescence as a mode of tumor suppression. Environ Health Perspect 1991;93:59–62.
29 O'Brien W, Stenman G, Sager R. Suppression of tumor growth by senescence in virally transformed human fibroblasts. Proc Natl Acad Sci USA 1986;83: 8659–8663.
30 Stevenson M, Volsky DJ. Activated v-myc and v-ras oncogenes do not transform normal human lymphocytes. Mol Cell Biol 1986;6:3410–3417.
31 Kang KS, Sun W, Nomata K, *et al.* Involvement of tyrosine phosphorylation of p185c-erbB2/neu in tumorigenicity induced by X-rays and the neu oncogene in human breast epithelial cells. Mol Carcinogen 1998;21:225–233.
32 Yoakum GH, Lechner JF, Gabrielson EW, *et al.* Transformation of human bronchial epithelial cells transfected by Harvey ras oncogene. Science 1985;227: 1174–1179.
33 Rhim JS, Jay G, Arnstein P, *et al.* Neoplastic transformation of human epidermal keratinocytes by AD12-SV40 and Kirsten sarcoma viruses. Science 1985;227: 1174–1179.
34 Hurlin PJ, Maher VM, McCormick JJ. Malignant transformation of human fibroblasts caused by expression of a transfected T24 HRAS oncogene. Proc Natl Acad Sci USA 1989;86:187–191.
35 Hahn WC, Weinberg RA. Rules for making human tumor cells. N Engl J Med 2002;347:1593–1603.
36 Hahn WC, Counter CM, Lundberg AS, *et al.* Creation of human tumour cells with defined genetic elements. Nature 1999;400:464–468.
37 Kim TM, Benedict WF, Xu HJ, *et al.* Loss of heterozygosity on chromosome 13 is common only in the biologically more aggressive subtypes of ovarian epithelial tumors and is associated with normal retinoblastoma gene expression. Cancer Res 1994;54: 605–609.
38 Yoo GH, Xu HJ, Brennan JA, *et al.* Infrequent inactivation of the retinoblastoma gene despite frequent loss of chromosome 13q in head and neck squamous cell carcinoma. Cancer Res 1994;54: 4603–4606.
39 Pei L, Melmed S, Scheithauer B, *et al.* Frequent loss of heterozygosity at the retinoblastoma susceptibility gene (RB) locus in aggressive pituitary tumors: evidence

for a chromosome 13 tumor suppressor gene other than RB. Cancer Res 1995;55:1613–1616.
40 Lai S, Benedict WF, Silver SA, *et al.* Loss of retinoblastoma gene function and heterozygosity at the RB locus in renal cortical neoplasms. Hum Pathol 1997;28:693–697.
41 Tamura K, Zhang X, Murakami Y, *et al.* Deletion of three distinct regions on chromosome 13q in human non-small-cell lung cancer. Int J Cancer 1997;74: 45–49.
42 Latil A, Chene L, Mangin P, *et al.* Extensive analysis of the 13q14 region in human prostate tumors: DNA analysis and quantitative expression of genes lying in the interval of deletion. Prostate 2003;57:39–50.
43 Solomou EE, Sfikakis PP, Kotsi P, *et al.* 13q Deletion in chronic lymphocytic leukemia: characterization of E4.5, a novel chromosome condensation regulator-like guanine nucleotide exchange factor. Leuk Lymphoma 2003;44:1579–1585.
44 Acikbas I, Keser I, Kilic S, *et al.* Detection of LOH of the RB1 gene in bladder cancers by PCR-RFLP. Urol Int 2002;68:189–192.
45 Mao L, Schoenberg MP, Scicchitano M, *et al.* Molecular detection of primary bladder cancer by microsatellite analysis. Science 1996;271:659–662.
46 Sourvinos G, Kazanis I, Delakas D, *et al.* Genetic detection of bladder cancer by microsatellite analysis of p16, RB1 and p53 tumor suppressor genes. J Urol 2001;165:249–252.
47 Steiner G, Schoenberg MP, Linn JF, *et al.* Detection of bladder cancer recurrence by microsatellite analysis of urine. Nat Med 1997;3:621–624.
48 Simoneau AR, Jones PA. Bladder cancer: the molecular progression to invasive disease. World J Urol 1994;12: 89–95.
49 Mark L, Jones P. Presence and location of TP53 mutations determines patterns of CDKN2A/ARF pathway in bladder cancer. Cancer Res 1998;58:5348–5353.
50 Knudson AG. Two genetic hits (more or less) to cancer. Nat Rev Cancer 2001;1:157–162.
51 Kleinerman RA, Tucker MA, Tarone RE, *et al.* Risk of new cancers after radiotherapy in long-term survivors of retinoblastoma: an extended follow-up. J Clin Oncol 2005;23:2272–2279.